Oncogene (2013), 1–10

www.nature.com/onc

ORIGINAL ARTICLE

Heparanase promotes lymphangiogenesis and tumor invasion in pancreatic neuroendocrine tumors

KE Hunter[1,2], C Palermo[1], JC Kester[1], K Simpson[1], J-P Li[3], LH Tang[4], DS Klimstra[4], I Vlodavsky[5] and JA Joyce[1]

Heparan sulfate proteoglycans are an important and abundant component of the extracellular matrix, which undergo substantial remodeling throughout tumorigenesis via the enzymatic activity of heparanase. Heparanase has been shown to be upregulated in many human cancers; however, its specific functions in human pancreatic neuroendocrine tumors (PanNETs) and spontaneous mouse models of cancer have not been evaluated. Here, we investigated the role of heparanase in PanNETs using patient samples and the RIP1-Tag2 (RT2) PanNET-transgenic mouse model. High heparanase expression significantly correlated with more advanced tumor stage, higher tumor grade and the presence of distant metastasis in PanNET patients. We genetically manipulated heparanase levels in the RT2 model using heparanase-transgenic mice, which constitutively overexpress heparanase, and heparanase-knockout mice. Heparanase was found to have a critical role in promoting tumor invasion, through both macrophage and cancer cell sources in the tumor microenvironment. In addition, elevated heparanase levels significantly increased peritumoral lymphangiogenesis *in vivo* and promoted the *trans*-differentiation of macrophages into lymphatic endothelial cell-like structures in culture. Conversely, we found that heparanase deletion led to increased angiogenesis and pericyte coverage. Together, these data identify important roles for heparanase in regulating several critical aspects of tumorigenesis, demonstrating that heparanase represents a potential therapeutic target for PanNET patients.

Oncogene advance online publication, 6 May 2013; doi:10.1038/onc.2013.142

Keywords: tumor microenvironment; tumor-associated macrophages; matrix-degrading enzyme; heparan sulfate proteoglycans

INTRODUCTION

Tumors develop in complex microenvironments comprising cancer cells surrounded by a diverse set of stromal cells and extracellular matrix (ECM) components.[1] The ECM is a heterogeneous mix of proteins and polysaccharides, including heparan sulfate proteoglycans (HSPGs), collagen, laminin and fibronectin, that form an intricate network. It functions as a scaffold for cell and tissue organization, providing important biochemical cues affecting cell function and differentiation. ECM remodeling is critical during multiple stages of tumor development, facilitating cancer cell proliferation, angiogenesis, invasion and metastasis.

HSPGs, which consist of a protein core with covalently attached heparan sulfate (HS) side chains, have important roles in these processes. The HS side chains bind to many growth factors, angiogenic proteins and chemokines, allowing HSPGs to function as storage depots for these factors.[2] HSPG processing is performed exclusively by heparanase, an endo-β-glucuronidase that cleaves HS side chains at specific intrachain sites, resulting in growth factor release.[2] Heparanase activity can thus lead to both physical remodeling of the ECM and the release of tethered growth factors, converting them to soluble bioactive mediators. These functions are consistent with reports of a significant correlation between high heparanase levels and poor patient prognosis in several tumor types.[2]

We have previously shown that heparanase is upregulated during multistage tumorigenesis in the RIP1-Tag2 (RT2) pancreatic neuroendocrine tumor (PanNET) model.[3] Treatment of RT2 mice with PI-88, a HS mimetic, resulted in impaired proliferation, angiogenesis and tumor invasion, indirectly implicating HS-mediated signaling and heparanase in regulating tumorigenesis. However, as PI-88 inhibits both heparanase and blocks the function of many HS-binding proteins, the specific contributions of the heparanase enzyme itself in pancreatic neuroendocrine tumorigenesis could not be directly addressed in this previous study.

PanNETs are a rare but clinically challenging tumor type, owing in part to marked disease heterogeneity and limited understanding of the underlying molecular mechanisms. PanNETs are the second most common pancreatic neoplasms, representing ~1.3% of pancreatic cancers in incidence and 10% of cases in prevalence.[4] Surgical resection is the most effective treatment option for PanNETs; however, ~65% of patients present with unresectable or metastatic disease. Patients with distant metastases have a median survival of only 24 months.[5] A recent exomic sequencing study of PanNETs identified mutations in genes encoding chromatin-remodeling subunits (DAXX/ATRX) and the MEN1 tumor suppressor,[6] which correlated with better patient prognosis. However, factors that are positively associated with poor PanNET prognosis critically still remain elusive. Given that heparanase expression correlates with worse prognosis in several other tumor types,[2] we decided to examine its importance in PanNETs and also its potential tumor-promoting roles in a spontaneous PanNET mouse model.

[1]Cancer Biology and Genetics Program, Memorial Sloan-Kettering Cancer Center, New York, NY, USA; [2]Louis V. Gerstner Jr. Graduate School of Biomedical Sciences, Memorial Sloan-Kettering Cancer Center, New York, NY, USA; [3]Department of Medical Biochemistry and Microbiology, Uppsala University, Uppsala, Sweden; [4]Pathology Department, Memorial Sloan-Kettering Cancer Center, New York, NY, USA and [5]Cancer and Vascular Research Center, Rappaport Faculty of Medicine, Technion, Israel. Correspondence: Dr JA Joyce, Cancer Biology and Genetics Program, Memorial Sloan-Kettering Cancer Center, 1275 York Avenue, Box 372, New York, NY 10065, USA.
E-mail: joycej@mskcc.org
Received 16 October 2012; revised 12 March 2013; accepted 14 March 2013

Here, we find that heparanase expression is significantly associated with increased malignancy and metastasis in PanNET patients. We genetically manipulated heparanase levels in the RT2 model using heparanase-transgenic mice, which constitutively overexpress heparanase, or heparanase-knockout mice, and identified critical roles for both macrophage- and cancer cell-derived heparanase in promoting tumor invasion. We found that heparanase deletion led to increased angiogenesis and enhanced pericyte coverage, potentially through activation of pericytes by HB-EGF. In addition, we showed that elevated heparanase activity induces tumor lymphangiogenesis *in vivo* and promotes the *trans*-differentiation of macrophages into lymphatic endothelial cell (LEC)-like structures in culture. Together, our findings demonstrate multifaceted roles for heparanase in supporting various processes critical to PanNET progression, and thus implicate heparanase as an attractive therapeutic target for PanNET patients.

RESULTS

Heparanase expression is associated with malignant progression in human PanNETs

We performed immunohistochemistry staining for heparanase protein on PanNET patient tissue samples and on normal islet samples. While normal islets had minimal heparanase levels, tumors exhibited positive staining that varied in intensity. We then obtained tissue microarrays (TMAs) with samples from over 150 PanNET patients, performed immunohistochemistry for heparanase and blindly scored for staining intensity on a 0 (no staining) to 3 (high staining) scale (Figure 1a). Comparing staining intensity with patient clinicopathological data revealed a significant correlation between increased heparanase staining score and higher tumor stage, as classified by the American Joint Committee on Cancer staging manual 7th edition,[7] and higher tumor grade as defined by tumor mitotic activity[8,9] (Figure 1b, Table 1). In addition, we found that an increased heparanase staining score in the primary tumor significantly correlated with the presence of distant metastasis (Table 1).

We next investigated whether heparanase messenger RNA (mRNA) was differentially expressed in primary tumors versus metastases. We isolated RNA from a separate cohort of matched samples of primary tumors and liver metastases, the most common metastatic site in PanNET patients. Heparanase expression was significantly upregulated by ~40-fold in primary tumors compared with normal islets, and was similarly expressed in matched primary and metastatic tumors (Figure 1c). Together, these data show that heparanase can function as an indicator for the aggressiveness of the primary tumor and distant metastasis in PanNET patients.

Genetic manipulation of heparanase levels in the RT2 PanNET model

To determine the specific roles that heparanase may have in promoting PanNET progression, we used the RT2 mouse model of islet cell carcinoma, which has proven very informative in studying neuroendocrine tumor progression, and in predicting clinical efficacy of new therapeutics.[10] We investigated the roles of heparanase during spontaneous tumorigenesis by genetically manipulating its level of expression in RT2 mice by crossing them to either heparanase-transgenic (*Hpa*-Tg) or heparanase-knockout (*Hpse* −/−) mice.[11,12] Both of these lines have been extensively analyzed, and no major developmental abnormalities have been identified.[11,12] *Hpa*-Tg mice express the human heparanase transgene under control of the β-actin promoter, leading to constitutive overexpression and increased heparanase activity of

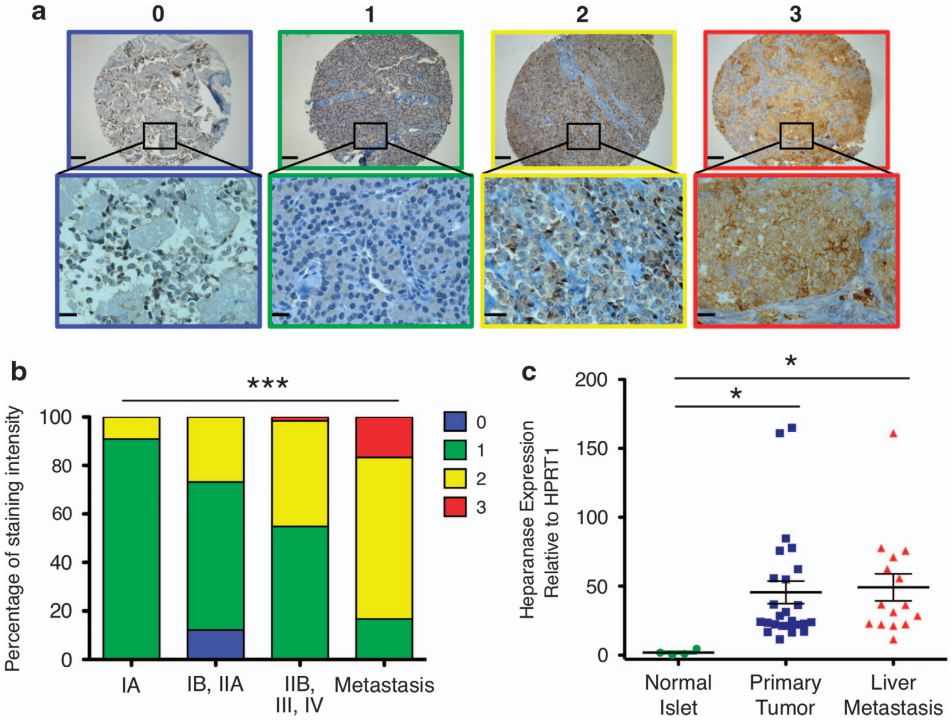

Figure 1. Heparanase expression is associated with malignant progression in human pancreatic neuroendocrine cancers. (**a**) Representative images for heparanase staining in TMAs constructed from PanNET patient samples. Heparanase staining intensity was scored on a 0 (absent staining) to 3 (high staining) scale. Scale bar for tissue sample overview: 100 μm, scale bar for inset: 20 μm. (**b**) Correlation of heparanase score with tumor stage by American Joint Cancer Committee staging manual 7th edition.[7] See Table 1 for detailed patient information, ***$P < 0.0001$, Fisher's exact test. (**c**) Heparanase expression, normalized to HPRT1, in mRNA from normal islets ($n = 4$), primary tumors ($n = 25$) and matched liver metastases ($n = 15$) from PanNET patients. Heparanase was significantly upregulated in primary tumors (*$P = 0.046$) and liver metastases (*$P = 0.026$) compared with normal islet samples. *P*-values in (**c**) were calculated by unpaired *t*-test.

Table 1. Comparison of clinical and histopathological parameters associated with increased levels of heparanase immunostaining in PanNET patients shown in Figure 1

Clinicopathological parameters	n	*Heparanase score*				P-*value**
		0	*1*	*2*	*3*	
Tumor grade						**0.008**
Low	87	6	64	17	0	
Intermediate	77	4	39	33	1	
High	3	0	1	2	0	
Staging (AJCC stage)						**<0.0001**
IA	22	0	20	2	0	
IB, IIA	82	10	50	22	0	
IIB, III, IV	61	0	33	27	1	
Metastasis	6	0	1	4	1	
Mitosis (per 50 HPFs)		1.5 ± 1.5	4.1 ± 1.6	10.85 ± 3.5	2.0	0.076
Distant metastasis						**0.022**
No metastasis	131	10	86	34	1	
Distant metastasis	37	0	19	18	0	

Abbreviations: AJCC, American Joint Cancer Committee; HPF, high-power field. Heparanase staining of tissue microarrays was correlated with clinicopathological parameters including AJCC tumor staging manual 7th edition,[7] tumor grade (low: <2 mitoses/50 HPF; intermediate: $\geqslant 2$ mitoses/50 HPF; high grade: >50 mitoses/50 HPF)[8] and the number of mitoses per 50 HPFs scored. Samples with incomplete patient data were excluded from some of the individual analyses. *The *P*-values were calculated by one-way analysis of variance for mitosis, and by Fisher's exact test for the other parameters. Significant *P*-values are indicated in bold.

6- to 30-fold, depending on the tissue examined.[12] When we analyzed end-stage mice at 13.5 weeks of age, we found that heparanase overexpression or deletion had no significant effect on tumor burden, assessed by both tumor size and tumor number (Figure 2a). Therefore, modulating levels of the heparanase enzyme did not impact PanNET initiation or growth.

We then determined whether the effects of heparanase manipulation could be observed by staining tissues for HS using the anti-HS antibody 10E4. In the tumor interior, HS staining was primarily localized to blood vessels (Figure 2b), which was expected, as HSPGs are abundant basement membrane components. HS staining was reduced in *Hpa*-Tg RT2 mice, indicative of increased turnover via heparanase processing. Consistent with this, we observed increased HS accumulation along blood vessels in *Hpse* $-/-$ RT2 mice. Interestingly, when specifically examining the invasive margin of wild-type (WT) RT2 tumors, HS levels were reduced, similar to *Hpa*-Tg RT2 tumors, indicating that heparanase was active at invasive edges in these tumors and degraded HS during the process of matrix remodeling and invasion.

Heparanase promotes PanNET invasion

The increased HS turnover observed at invasive tumor fronts led us to investigate whether genetic manipulation of heparanase levels affected tumor invasion. Tumors were graded histologically into three classes: encapsulated tumors, microinvasive tumors (IC1) and frankly invasive carcinomas (IC2).[13] While the total number of tumors did not change in any of the genotypes (Figure 2a), *Hpa*-Tg RT2 mice had significantly more invasive carcinomas compared with WT RT2, with a pronounced 250% increase in the IC2 class (Figure 2c). Conversely, deletion of heparanase led to significantly less invasive tumors, consistent with an important role for heparanase in promoting tumor invasion (Figure 2c). While it has been proposed that heparanase functions in ECM remodeling,[2] this is the first time that the striking effects of heparanase on regulating invasion have been reported in a spontaneous tumor model.

Having established that heparanase has an important role in promoting PanNET invasion, we were interested in further characterizing which cell types within the tumor microenvironment were a source of heparanase and were functionally important for tumor invasion. We isolated cancer cells, tumor-associated macrophages (TAMs) and endothelial cell populations from WT mice by FACS. We found that heparanase was expressed in cancer cells and was further enriched in TAMs (Figure 2d). Previous analysis of macrophage density in human PanNET samples revealed a significant, positive correlation with poor prognosis and metastasis, implicating TAMs in PanNET tumorigenesis.[14] In addition, studies in the RT2 model have shown that TAM-supplied cysteine cathepsins have critical roles in tumorigenesis,[15] leading us to question whether TAM-supplied heparanase was similarly important for promoting tumor invasion.

TAM- and cancer cell-supplied heparanase promote tumor invasion

To functionally test the importance of heparanase in TAMs versus cancer cells, we undertook bone marrow (BM) transplantation studies. Previous work has shown that in the RT2 model, 88% of BM-derived cells (BMDCs) found in tumors are TAMs.[15] Therefore, BM transplantation provides a means to genetically manipulate TAM-supplied heparanase levels in RT2 tumors. We transplanted BM isolated from either *Hpa*-Tg or *Hpse* $-/-$ mice, which were also positive for actin-green fluorescent protein, into lethally irradiated WT RT2 mice. Mice were aged to 13.5 weeks and analyzed for tumor burden and tumor invasion. As in the non-BMT genotypes (Figure 2a), there was no impact of BM transplantation of the different heparanase genotypes on tumor burden (data not shown). However, we found that transplantation of *Hpse* $-/-$ BM into WT RT2 mice significantly decreased tumor invasion, compared with the WT BM transplantation control (Figure 2e), indicating that TAM-supplied heparanase indeed has a critical role in promoting tumor invasion. Interestingly, analysis of WT RT2 mice transplanted with *Hpa*-Tg BMDCs did not show an increase in tumor invasion over the WT BM control, suggesting that the already high levels of heparanase in TAMs from WT RT2 tumors (Figure 2d) are sufficient to promote tumor invasion. These analyses also indicate that cancer cell-supplied heparanase (or heparanase derived from a minor non-BM-derived stromal cell type) has some role in enhancing invasion, as transplantation of *Hpa*-Tg BMDCs into WT RT2 tumors did not recapitulate the higher proportion of invasive tumors observed in the constitutive *Hpa*-Tg RT2 mice (Figure 2c). Therefore, heparanase promotes tumor invasion through both TAMs and cancer cells.

Heparanase deletion leads to enhanced angiogenesis

As heparanase expression has been shown to enhance tumor angiogenesis in other contexts,[2] we investigated the effects of genetic manipulation of heparanase levels on blood vessel density in the RT2 model. Using the endothelial cell marker CD31, we quantitated the total blood vessel area in tumor sections from WT RT2, *Hpa*-Tg RT2 and *Hpse* $-/-$ RT2 mice (Figure 3a). Surprisingly, we found that while WT RT2 and *Hpa*-Tg RT2 mice showed comparable tumor angiogenesis, *Hpse* $-/-$ RT2 mice had a 1.7-fold increase in vessel area (Figure 3b). We also investigated the pericyte coverage of the blood vessels as measured by the percentage of the pericyte marker NG2 overlapping with CD31. We found that *Hpse* $-/-$ RT2 mice also exhibited a significant increase in pericyte coverage. This was not simply the consequence of increased angiogenesis, as there was a further 1.8-fold increase in pericyte numbers when normalized to blood vessel number, compared with WT RT2 and *Hpa*-Tg mice (Figure 3b).

The increased angiogenesis observed in the *Hpse* $-/-$ RT2 mice was unexpected, as heparanase has been described to have a proangiogenic role, in part owing to its release of soluble

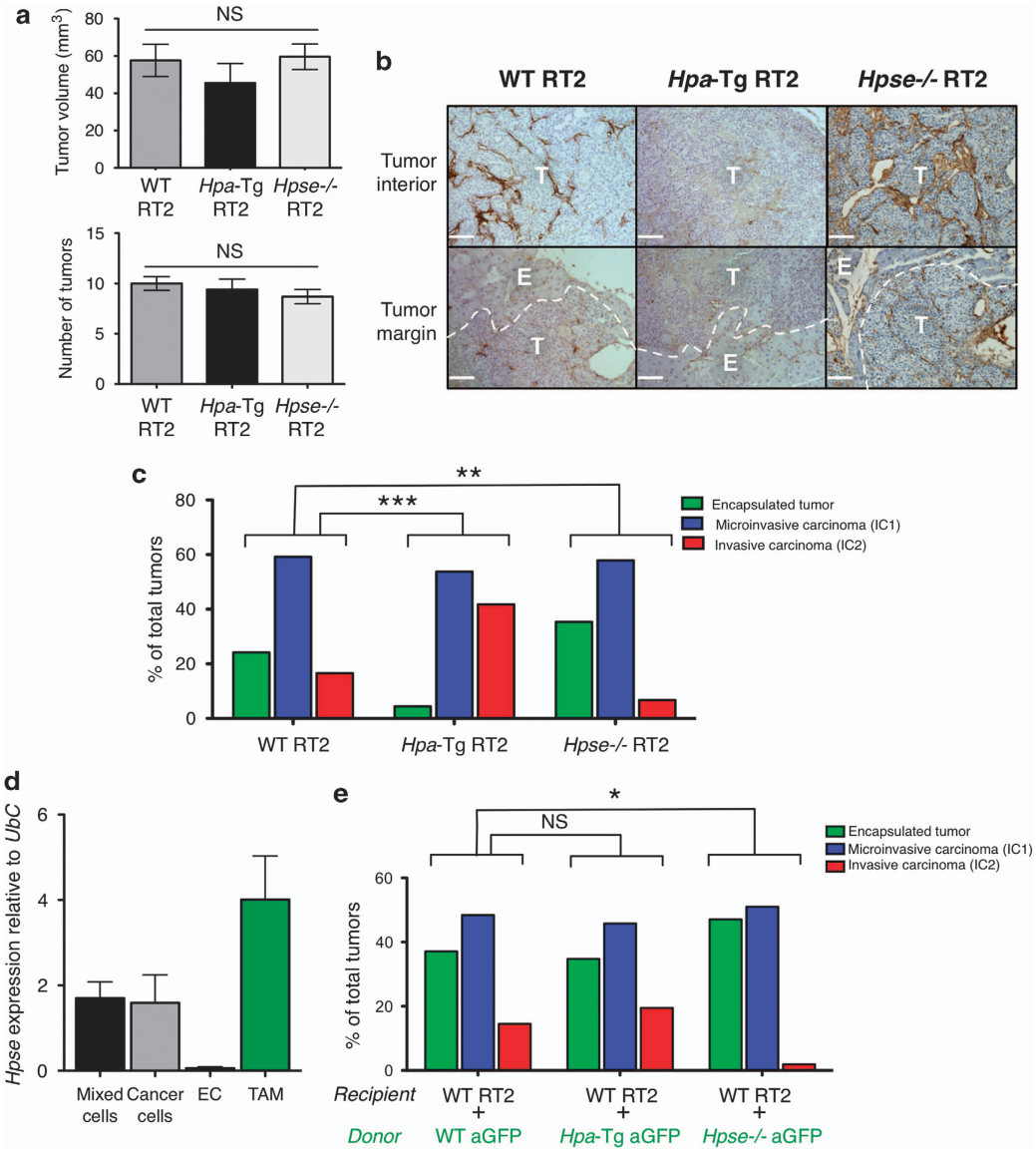

Figure 2. Genetic loss or gain of heparanase function contributes to invasion through both TAM and cancer cell-derived sources. (**a**) Tumor burden was determined in WT RT2 ($n=40$), *Hpa*-Tg RT2 ($n=25$) and *Hpse* $-/-$ RT2 ($n=26$) mice at 13.5 weeks of age. There was no significant (NS) difference in tumor volume or tumor number for either genotype compared with WT RT2. (**b**) Paraffin sections of WT RT2, *Hpa*-Tg RT2 and *Hpse* $-/-$ RT2 mice were stained for HS (brown). Scale bar: 50 μm. White dotted line indicates the margin between the tumor (T) and surrounding normal exocrine (E) pancreas. (**c**) Hematoxylin and eosin (H&E) staining was used to grade tumors in WT RT2 ($n=30$), *Hpa*-Tg RT2 ($n=10$) and *Hpse* $-/-$ RT2 ($n=10$) mice. The relative proportions of encapsulated, microinvasive (IC1) and invasive carcinomas (IC2) were graphed. There was a significant increase in invasion in *Hpa*-Tg RT2 mice compared with WT RT2 (***$P<0.001$), and a significant decrease in invasion in *Hpse* $-/-$ RT2 mice compared with WT RT2 (**$P=0.004$). (**d**) WT RT2 tumors were sorted by flow cytometry into total mixed cells, cancer cell, endothelial cell (EC) and TAM fractions, and expression of heparanase by quantitative reverse transcriptase PCR was determined. Heparanase expression was normalized relative to ubiquitin C (Ubc) levels. $n=4$ independent experiments. (**e**) H&E staining was used to grade tumors following BM transplantation of WT aGFP ($n=10$), *Hpa*-Tg aGFP ($n=13$) or *Hpse* $-/-$ aGFP ($n=7$) BM into WT RT2 mice. There was a significant decrease in tumor invasion in *Hpse* $-/-$ BM transplanted into WT RT2 mice (*$P=0.02$). *P*-values were calculated using an unpaired *t*-test in (**a**), and a cumulative logit model[30] in (**c**) and (**e**).

proangiogenic growth factors such as VEGF-A. Given the increase in HS levels along blood vessels in the *Hpse* $-/-$ RT2 mice (Figure 2b), we hypothesized that this HS could instead act to locally concentrate HS-binding growth factors and thus enhance angiogenesis. Previous work in the RT2 model has shown that the heparin binding EGF-like growth factor HB-EGF is an important activator of epidermal growth factor receptor (EGFR) signaling in pericytes, increasing pericyte coverage and supporting angiogenesis.[9] As these phenotypes are very similar to those observed here in the *Hpse* $-/-$ RT2 tumors, we investigated whether activation of EGFR, as a read-out of HB-EGF binding, was altered in *Hpse* $-/-$ RT2 mice. Indeed, we observed increased phospho- (p)EGFR staining in tumors from *Hpse* $-/-$ RT2 mice, as compared with WT RT2 or *Hpa*-Tg mice (Figure 3c). This staining was localized to cells adjacent to MECA32^{+} endothelial cells, which is consistent with the localization of pericytes. Co-staining with the pericyte marker NG2 confirmed that pEGFR staining was present in pericytes (Figure 3d). Therefore, increased local signaling and the resulting activation of

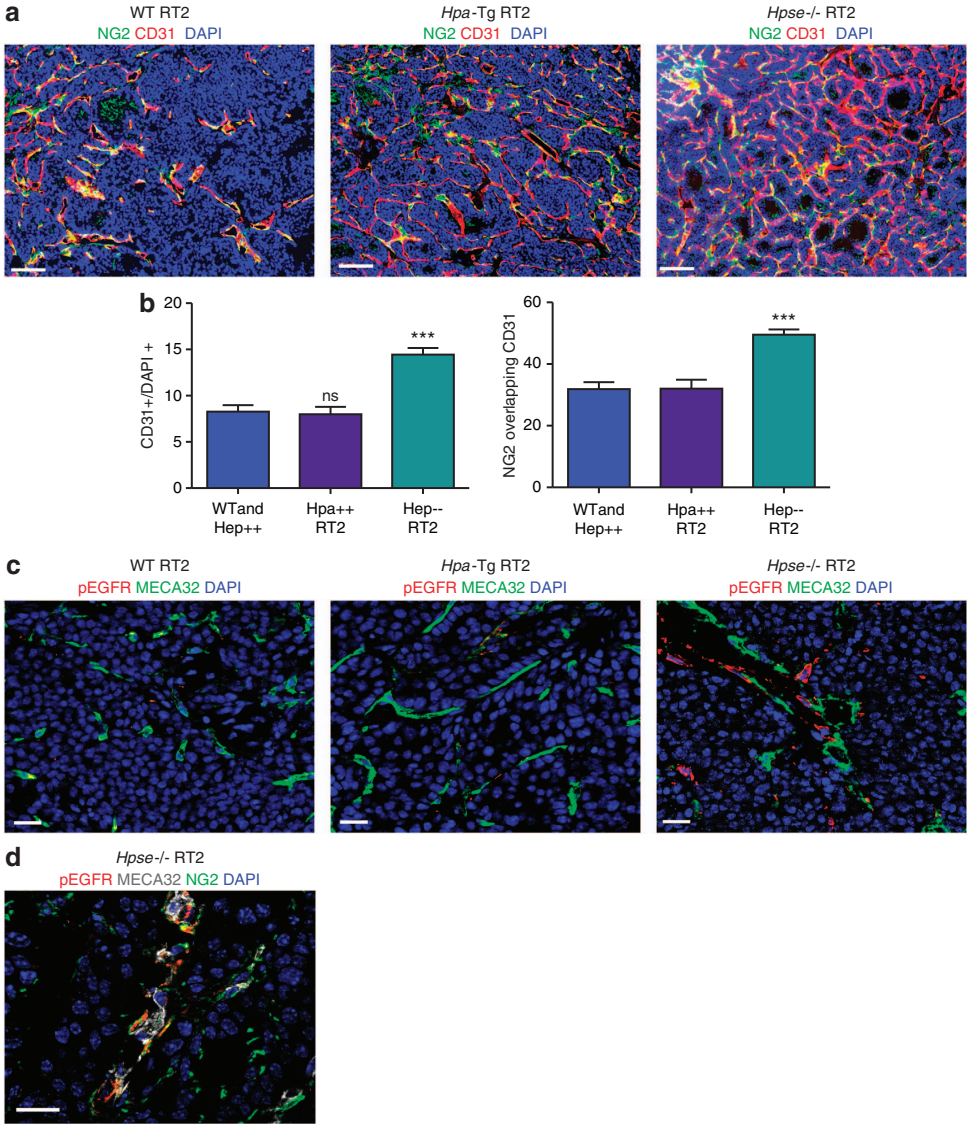

Figure 3. Heparanase deletion leads to increased angiogenesis and pericyte coverage. (**a**) Representative images from tumors stained with CD31 (endothelial cells), NG2 (pericytes) and DAPI (nuclei). Scale bar: 100 μm. (**b**) Quantitation of the total CD31 area, normalized to DAPI area, and the percentage of NG2 that is overlapping CD31 (pericyte coverage) were calculated using MetaMorph. *Hpse* −/− RT2 mice exhibited significantly more blood vessels and increased pericyte coverage. Statistics were calculated using an unpaired *t*-test; ***$P<0.001$, NS, not significant. (**c**) Representative images of pEGFR (Tyr1068) staining in WT RT2, *Hpa*-Tg RT2 and *Hpse* −/− RT2 tumors, with MECA32 staining endothelial cells. Scale bar: 20 μm. (**d**) Representative image depicting pEGFR staining in NG2-positive pericytes in a *Hpse* −/− RT2 tumor. Scale bar: 20 μm.

pericytes by HB-EGF is one potential explanation for the increased angiogenesis and pericyte coverage in *Hpse* −/− RT2 mice.

Heparanase overexpression enhances lymphangiogenesis

Given the roles we have identified for heparanase in promoting malignancy, we were interested in investigating whether other aspects of tumorigenesis were affected by manipulating heparanase levels. Examination of pancreatic tissue sections from *Hpa*-Tg RT2 mice indicated a pronounced increase in peritumoral lymphangiogenesis, visualized by staining with the lymphatic endothelial marker LYVE-1 (Figure 4a). Co-staining with the macrophage marker F4/80 confirmed that these were lymphatic vessels and not LYVE-1$^+$ macrophages. Quantitation of peritumoral lymphatics revealed a 2.5-fold increase in lymphatic vessel area in *Hpa*-Tg RT2 mice compared with WT RT2 mice (Figure 4b). In addition, we found a 3.2-fold increase in the lymphatic vessel density in the peritumoral region of *Hpa*-Tg RT2 mice (Figure 4c), indicating that there is an increase in the number of lymphatic vessels, not simply an expansion of pre-existing vessels. Analysis of *Hpse* −/− RT2 mice showed a comparable number of lymphatic vessels and a similar vessel area to WT RT2 (Figure 4b, c), indicating that while heparanase overexpression induces additional lymphangiogenesis, it is not required for the basal level of peritumoral lymphatic vessels seen in WT RT2 mice. We also examined whether there was any association between increased tumor invasion and lymphangiogenesis in the *Hpa*-Tg mice, but found lymphatic vessels in association with both invasive and encapsulated tumors in all genotypes.

Previous studies have shown that overexpression of VEGF-C in a β-cell-specific manner led to increased peritumoral lymphangiogenesis in RT2 mice.[16] We found no increase in the expression of

VEGF-C, or other pro-lymphangiogenic growth factors, in total tumor RNA or in sorted tumor cell populations from *Hpa*-Tg mice (Supplementary Figure S1). This result indicates that changes in mRNA expression do not underlie this phenotype, but instead implicate heparanase-mediated growth factor release in promoting lymphangiogenesis. In addition, in RT2 tumors, we frequently observed a close association of F4/80$^+$ macrophages and lymphatic vessels (Figure 4d). Myeloid cells have been shown to have important roles in lymphangiogenesis, through secretion of pro-lymphangiogenic growth factors or by direct incorporation into lymphatic vessels.[17] Given the high heparanase expression in TAMs, we were therefore interested in determining the impact of heparanase overexpression in macrophages in the context of lymphangiogenesis. Previous studies have shown that macrophages can be induced to *trans*-differentiate into lymphatic endothelial-like cells,[18,19] and thus we investigated whether heparanase overexpression enhanced this process.

BM was isolated from WT or *Hpa*-Tg mice, and differentiated into BM-derived macrophages (BMDMs) in culture using colony-stimulating factor-1. These cells were plated on a mixture of Matrigel and LEC media, and incubated for up to 8 days. As shown previously,[19] macrophages clustered together and formed LEC-like structures. Interestingly, *Hpa*-Tg BMDM showed an increased number and size of these structures at the end of the assay (Figure 5a), and expressed the LEC-specific marker podoplanin (Figure 5b). To further characterize these structures, we isolated RNA from cells at either the establishment of the cultures or after 8 days of culture when mature structures had formed. We saw no significant difference in any marker at day 0 between WT and *Hpa*-Tg BMDM (Figure 5c). As expected, the *Hpa*-Tg cultures at day 8 trended toward increased expression of the LEC markers *LYVE-1*, *podoplanin* and *VEGFR-3* (Figure 5c). We observed a concordant decrease in *VEGFR-1* and *VEGFR-2* at day 8.

We found a significant elevation in the expression of the growth factors *VEGF-C*, *VEGF-D* and *FGF-2*, which are all pro-lymphangiogenic[20] (Figure 5c). However, there was no increase in *VEGF-A* or *HGF* mRNA expression, which have also been reported to promote lymphangiogenesis.[20] To test whether these growth factors were able to increase lymphatic structure formation, individual recombinant proteins were added to the assay, and the total

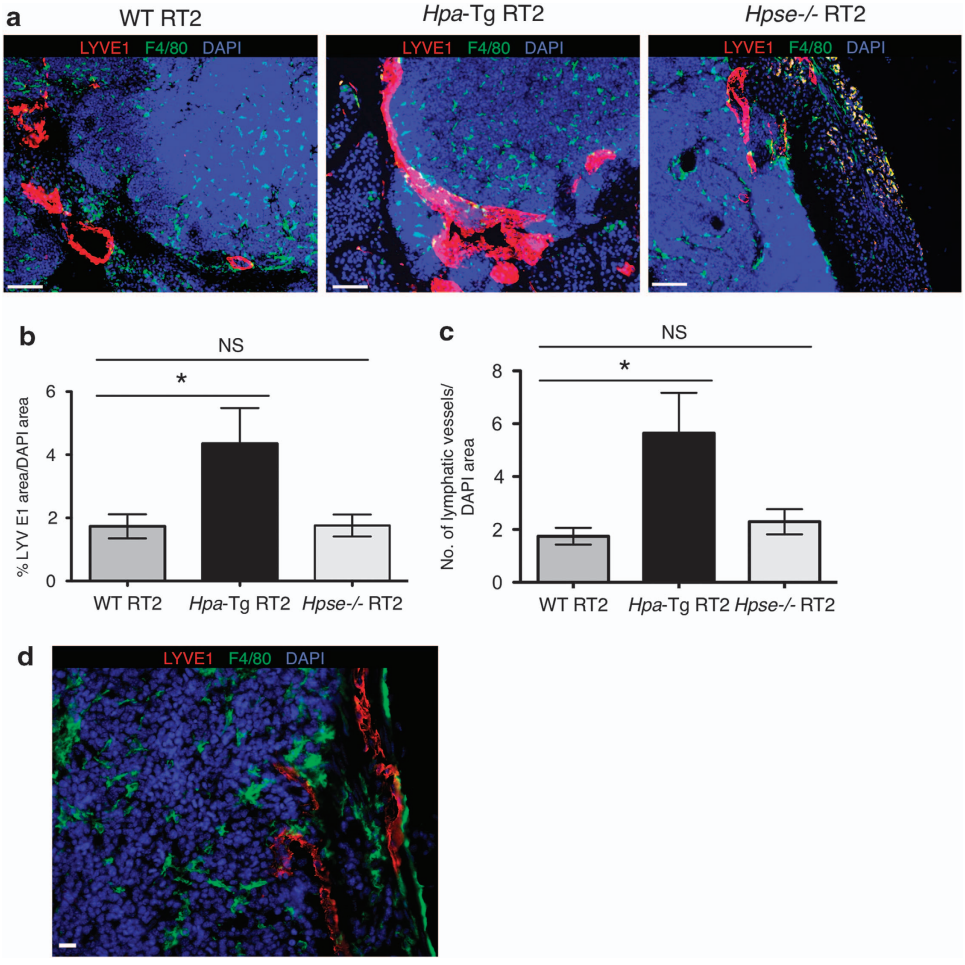

Figure 4. Enhanced peritumoral lymphangiogenesis in *Hpa*-Tg RT2 mice. (**a**) Representative images showing increased lymphangiogenesis in *Hpa*-Tg mice, compared with WT RT2 and *Hpse* $-/-$ RT2. Thirty-five-micrometer frozen sections were stained for LYVE-1 (red), F4/80 (green) and DAPI (blue). Scale bar: 100 μm. (**b**) Lymphatic vessel area was quantitated in an area 500 μm in peritumoral diameter using MetaMorph software. Total LYVE-1$^+$ area was divided by total DAPI$^+$ area. *Hpa*-Tg RT2 mice had significantly increased lymphangiogenesis compared with WT RT2 mice; **P* = 0.039 by unpaired *t*-test. WT RT2 and *Hpa*-Tg RT2, *n* = 12 mice; *Hpse* $-/-$ RT2, *n* = 6 mice. (**c**) Lymphatic vessel density was quantitated in an area 500 μm in peritumoral diameter by counting the number of LYVE-1$^+$ vessels and dividing by the area of the peritumoral region. The increase in lymphangiogenesis was the result of the appearance of additional vessels, not a simple expansion of large lymphatic spaces. **P* = 0.02 by unpaired *t*-test compared with WT RT2 mice. (**d**) Representative image showing F4/80$^+$ macrophages (green) in close proximity to LYVE-1$^+$ lymphatic vessels (red) in a *Hpa*-Tg RT2 tumor. Scale bar: 20 μm.

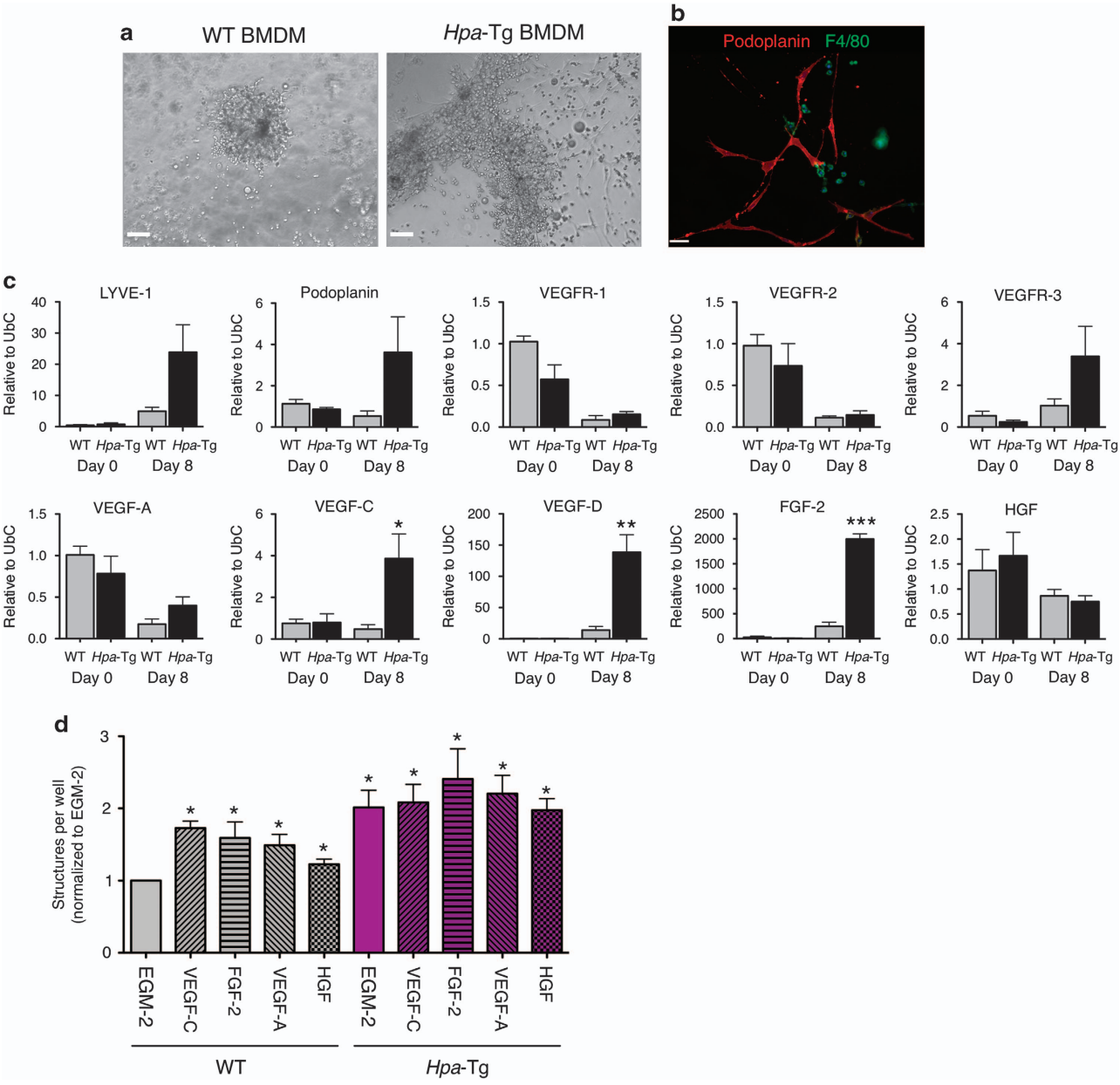

Figure 5. *Hpa*-Tg macrophages show increased *trans*-differentiation into lymphatic-like structures. (**a**) Representative day 8 cultures of BMDM plated on Matrigel and EGM-2. Scale bar: 100 μm. (**b**) Representative immunofluorescence staining for podoplanin and F4/80 on day 8 *Hpa*-Tg cultures. Scale bar: 100 μm. (**c**) Quantitative reverse transcriptase PCR analysis of day 0 and day 8 cultures. mRNA was isolated from cells plated in 24-well dishes and expression analysis determined for the genes listed, relative to ubiquitin C. At day 8, *Hpa*-Tg cultures showed a significant upregulation of VEGF-C (*$P = 0.029$), VEGF-D (**$P = 0.005$) and FGF-2 (***$P < 0.0001$) by unpaired *t*-test. $n = 4$ independent experiments. (**d**) Growth factors were added to cultures and number of LEC-like structures were counted at day 8 and normalized to the WT EGM-2 condition for each experiment ($n = 3$–4 repeat experiments per growth factor). The source of cells (WT or *Hpa*-Tg) is indicated below. *$P < 0.05$ compared with WT EGM-2 using the Mann–Whitney test.

number of structures counted at day 8. VEGF-C and FGF-2 increased the number of structures formed in the WT condition, to levels seen with *Hpa*-Tg BMDM (Figure 5d), with somewhat less pronounced increases for VEGF-A and HGF. However, there was no further increase in structure formation when these factors were added to *Hpa*-Tg cells, indicating they are already at sufficiently high levels in this experimental condition. Therefore, heparanase overexpression increases the ability of BMDM to form LEC-like structures in culture through a process that may be owing to their increased production/enhanced bioavailability of pro-lymphangiogenic growth factors. It was not possible to determine whether this enhanced *trans*-differentiation also occurred *in vivo,* which is an interesting question to address in future studies.

DISCUSSION

PanNETs are a clinically challenging tumor type, owing to marked disease heterogeneity and a limited understanding of the molecular basis for their development. We found that while heparanase mRNA is expressed at very low levels in normal islets,

its expression is increased 40-fold in primary tumors and metastatic tumors. Moreover, elevated heparanase levels in the primary tumor were significantly correlated with increased malignancy and the presence of metastatic disease (Table 1). These data indicate that heparanase levels increase in primary tumors that have the propensity to metastasize, and remain highly expressed in tumor cells that successfully colonize distant organs, including the liver. These results also suggest there is no advantage of further upregulating heparanase mRNA expression in metastases, as it is already expressed at a sufficiently high level. Our results thus identified heparanase as an intriguing therapeutic target for PanNETs and led us to further investigate the molecular mechanisms by which heparanase promotes tumorigenesis.

We turned to the well-characterized RT2 model of pancreatic islet carcinoma to investigate the specific roles of heparanase in tumor progression. Previous work using the HS mimetic PI-88 had indirectly implicated both heparanase and HS-mediated signaling in RT2 tumorigenesis.[3] However, PI-88 has much broader effects than simply inhibiting heparanase activity; it also sequesters HS-binding factors,[21] of which there are many,[22,23] thereby regulating their bioavailability and activity. Because of these broad inhibitory effects of PI-88, here we used a genetic approach to modulate heparanase levels, as this allowed us to specifically examine the contribution of heparanase alone to RT2 tumorigenesis. Utilization of *Hpa*-Tg mice, which overexpress heparanase, and *Hpse* $-/-$ mice, in which heparanase is deleted, enabled us to genetically modulate heparanase levels in a spontaneous mouse model of cancer for the first time.

While heparanase has previously been described to increase cancer invasion in cell lines,[24] we have now shown that heparanase expression dramatically enhanced tumor invasion in a spontaneous tumor model. We found that overexpression of heparanase led to a 2.5-fold increase in the most invasive class of tumors and that deletion of heparanase resulted in a significant decrease in tumor invasion. We propose that the increase in tumor invasion modulated by heparanase is at least partially a result of ECM degradation, demonstrated by decreased HS levels at the invasive fronts of tumors. Consistently, the overall decrease in HS levels in the *Hpa*-Tg RT2 tumors and the increased levels in the *Hpse* $-/-$ RT2 tumors demonstrates the activity of heparanase in HS remodeling.

Using BM transplantation studies, we found that TAM-supplied heparanase promoted invasion, as removal of heparanase from BMDCs significantly impaired tumor invasion. Interestingly, we observed that transplantation of *Hpa*-Tg BM into WT RT2 mice was not sufficient to increase invasion to the levels seen in the constitutive *Hpa*-Tg mice, also implicating a non-BMDC population in invasion. We hypothesize that these cells are cancer cells, as they make up the majority of the tumor bulk, though it is also formally possible that heparanase supplied by another non-BM-derived stromal cell type could be influencing tumor invasion. However, we have only detected heparanase expression in TAMs and cancer cells, arguing against the involvement of any other stromal cell type. Therefore, we conclude that heparanase promotes tumor invasion through both TAM-derived and cancer cell-derived sources.

Interestingly, we found that genetic modulation of heparanase levels had differential effects on blood vessels and lymphatic vessels, whereas several reports have ascribed positive roles for heparanase in both of these processes. While *Hpa*-Tg RT2 mice exhibited increased peritumoral lymphangiogenesis, *Hpse* $-/-$ RT2 mice unexpectedly showed increased tumor angiogenesis. Analysis of growth factors involved in these processes revealed no differences in mRNA expression levels, suggesting an important role for heparanase in regulating growth factor release from HSPG depots. The opposing phenotypes observed in these mice underscore the complexity of matrix remodeling and homeostasis. This suggests that the balance of increased soluble growth factor release mediated by heparanase overexpression can be countered by HS accumulation and potential increases in local HS signaling.

Heparanase has been implicated in promoting angiogenesis, through release of proangiogenic growth factors such as VEGF-A.[2] Surprisingly, we found no increase in angiogenesis in *Hpa*-Tg RT2 mice, but rather an increase in *Hpse* $-/-$ RT2 mice. In the RT2 model, cancer cells produce high levels of VEGF-A and thus VEGF-A signaling may already be saturated, with any increase in the bioavailability of VEGF-A by heparanase overexpression having a negligible effect. However, the increased accumulation of HS along the vessels in *Hpse* $-/-$ RT2 mice raised the interesting possibility that it was acting as a local, concentrated sink for heparin-binding growth factors and thus activating the vasculature. Previous work in the RT2 model showed that one such factor, HB-EGF, has an important role in activating pEGFR on pericytes, leading to increased pericyte coverage and support of angiogenesis.[9] Consistent with this, we observed increased pEGFR staining in *Hpse* $-/-$ RT2 mice and a significant increase in pericyte coverage. These results are also in accordance with studies showing that pericyte recruitment engages either cell-autonomous or endothelial cell-associated HS-bound PDGF-B to activate PDGFR-β signaling.[25]

The striking increase in lymphatic vessel number observed in *Hpa*-Tg RT2 mice was intriguing, as a previous study in head and neck cancer showed that heparanase expression correlated with lymphatic vessel density in patients.[26] It has also been reported that heparanase overexpression in cell lines leads to an increase in expression of VEGF-C, a pro-lymphangiogenic growth factor.[26] However, expression analysis of VEGF-C in whole RT2 tumors showed no significant differences between the three genotypes indicating that the elevated lymphangiogenesis seen in *Hpa*-Tg RT2 mice was not owing to increased mRNA expression of VEGF-C. Given the importance of heparanase in releasing ECM-tethered growth factors,[2] it is possible that increased heparanase levels leads to more bioactive VEGF-C, which then promotes lymphangiogenesis in the *Hpa*-Tg mice.

We additionally investigated the role of myeloid cells in this process, given their importance in lymphangiogenesis and the close association of macrophages with lymphatic vessels observed in RT2 tumors[17] (Figure 4c). We found that heparanase overexpression enhanced the ability of macrophages to *trans*-differentiate into LEC-like structures in culture. This *trans*-differentiation was accompanied by increased expression of lymphangiogenic markers and pro-lymphangiogenic growth factors. This increased expression could be owing to the higher expression by *trans*-differentiated cells, of which there are more in the *Hpa*-Tg cultures, or heparanase could in fact be driving this *trans*-differentiation. To begin to interrogate this, we added lymphangiogenic growth factors to the media of cultures, and found that this was able to increase the number of LEC-like structures in WT cultures to similar levels seen in the *Hpa*-Tg group. However, growth factor addition did not further increase the number of structures in the *Hpa*-Tg group, indicating that growth factor levels or signaling were at sufficiently high levels in this experimental condition. Our results are consistent with a model in which heparanase overexpression leads to increased release and bioavailability of VEGF-C, thereby activating lymphangiogenesis. In addition, myeloid cells that overexpress heparanase may help to support this lymphangiogenesis, either through direct incorporation into lymphatic vessels as has been shown in previous studies,[18] or by increased production of pro-lymphangiogenic growth factors.

In conclusion, our studies have revealed multiple novel functions for heparanase in enhancing pancreatic neuroendocrine tumorigenesis. Using complementary genetic approaches, we found that heparanase overexpression induces lymphangiogenesis *in vivo* and promotes *trans*-differentiation of macrophages into LEC-like structures in culture. Surprisingly, deletion of

heparanase increased tumor angiogenesis in RT2 mice, thus highlighting the complexity of the roles that matrix-remodeling enzymes have in tumorigenesis. In addition, we showed that heparanase produced by both TAMs and cancer cells is important in promoting tumor invasion. Our results from the RT2 model are especially relevant, as we have also shown that heparanase expression significantly correlates with increased malignancy in patients with PanNETs. Therefore, heparanase represents an attractive therapeutic target for PanNET patients.

MATERIALS AND METHODS

Transgenic mice

The generation and characterization of RT2,[27] *Hpa*-Tg[12] and *Hpse* $-/-$ [11] mice have been previously reported. *Hpse* $-/-$ and *Hpa*-Tg mice were backcrossed to the C57BL/6 background for at least 10 generations. β-Actin-green fluorescent protein-transgenic mice[28] in the C57BL/6 background were purchased from Jackson Laboratories (Bar Harbor, ME, USA). BM transplantation experiments were performed as previously described.[15]

Tissue processing and analysis

RT2 mice were killed by heart perfusion with phosphate-buffered saline followed by 10% zinc-buffered formalin. Tumor-containing pancreas and control tissues were removed, placed in 30% sucrose overnight and embedded in optimum cutting temperature (Tissue-Tek, Torrance, CA, USA) or were formalin-fixed overnight, processed through an ethanol series and embedded in paraffin blocks. Lesions greater than $1 \times 1\,mm^2$ were counted as tumors. Tumor burden was represented as the sum of the volumes of all tumors per mouse and calculated using the formula: volume = width^2 × length × 0.52 to approximate the volume of a spheroid. Frozen sections (10 μm or 35 μm thickness) were cut on a cryostat and paraffin sections (5 μm) were cut on a microtome. For invasion grading, hematoxylin and eosin staining was performed and the lesions were graded as previously described,[13] following a double-blind protocol and independently assessed by two investigators (KEH and JAJ).

Immunostaining of tissue sections

For immunofluorescence staining of 10-μm-thick frozen sections, slides were blocked with 1 × PNB-blocking buffer (Perkin Elmer, Waltham, MA, USA), incubated with the primary antibody of interest overnight at 4 °C, incubated with the corresponding fluorescently tagged secondary antibody for 1 h at room temperature, incubated with 4,6-diamidino-2-phenyl indole (DAPI) for 10 min and mounted with ProLong Gold (Invitrogen, Grand Island, NY, USA). For immunofluorescence on 35 μm sections, slides were permeabilized with 0.3% Triton X, blocked with 5% goat serum, incubated with primary antibodies overnight at room temperature, incubated with corresponding fluorescently tagged secondary antibody for 4.5 h at room temperature, incubated with DAPI for 20 min and mounted with ProLong Gold. Paraffin sections were stained using diaminobenzidine detection with a Discovery XT automated staining processor (Ventana Medical Systems Inc., Oro Valley, AZ, USA). Tissue sections were visualized under a Carl Zeiss (Thornwood, NY, USA) Axioimager Z1 microscope equipped with an Apotome. The following antibodies were used for immunofluorescence: rat anti-CD31 (BD, San Jose, CA, USA 1:100), rat anti MECA32 (BD, 1:100), rabbit anti-NG2 (Millipore, Billerica, MA, USA, 1:200), mouse anti-pEGFR (Tyr1068, Cell Signaling, Danvers, MA, USA, 1:100), rabbit anti-LYVE-1 (Abcam, Cambridge, MA, USA, 1:500), rat anti-F4/80 (Serotec, Raleigh, NC, USA, 1:1000) and Syrian hamster anti-podoplanin (AngioBio, Del Mar, CA, USA, 1:500). The following antibodies were used for diaminobenzidine staining: mouse anti-HS (10E4, Seikagaku Corp, Tokyo, Japan, 1:200) and rabbit anti-human heparanase (gift from I Vlodavsky, 1:500;[26]). Stained tissue sections were acquired using TissueFAXS software (TissueGnostics, Tarzana, CA, USA). Analysis of tumor vasculature was performed by calculating total MECA32 area, total DAPI area and the area of NG2 that overlapped MECA32 with MetaMorph (Sunnyvale, CA, USA) analysis software. Lymphangiogenesis analysis was performed on 35 μm sections using MetaMorph software (Molecular Devices, Sunnyvale, CA, USA) using a dilated peritumoral region, 500 μm in diameter, to calculate the total LYVE-1$^+$ area and the total DAPI$^+$ area within this region. Lymphatic vessel density measurements were calculated by counting the number of discrete lymphatic vessels in a 500 μm peritumoral area, and dividing by the total DAPI$^+$ peritumoral area.

Assay for *trans*-differentiation of BMDM into LEC-like structures

Femurs and tibiae from WT or *Hpa*-Tg mice, in the C57BL/6 background, were harvested under sterile conditions from both legs and flushed using a 25-gauge needle. The marrow was passed through a 40 μm strainer and cultured in 30 ml Teflon bags (PermaLife, Austin, TX, USA) with 10 ng/ml recombinant mouse colony-stimulating factor-1 (R&D Systems, Minneapolis, MN, USA). BM cells were cultured in Teflon bags for 7 days, with fresh colony-stimulating factor-1-containing medium replacing old medium every other day to induce macrophage differentiation. Matrigel (Becton Dickenson, Franklin Lakes, NJ, USA) and endothelial cell media EGM-2 MV (Lonza, Allendale, NJ, USA) were mixed 1:1 and plated on 24- or 96-well plates for 1 h at 37 °C. BMDM were collected and either 8×10^4 (96-well) or 5×10^5 (24-well) cells were plated per well in EGM-2 supplemented with 1 μg/ml lipopolysaccharide. After 8 days of culture, cells were isolated by washing with ice-cold phosphate-buffered saline and lysing in TRIzol reagent (Invitrogen) for RNA isolation. For assays with growth factor addition, BMDM were plated with four replicates in 96-well plates with EGM-2 supplemented with either 100 ng/ml mouse VEGF-A^{164} (R&D Systems), mouse VEGF-C (Sigma, St Louis, MO, USA), mouse FGF-2 (R&D Systems) or mouse HGF (R&D Systems) and replenished at day 3 of culture. At day 8 of culture, wells were visualized and number of LEC-like structures were counted and normalized within each experiment. Immunofluorescence analysis of LEC-like structures was performed on cultures at day 8 using DAPI, anti-podoplanin and anti-F4/80 antibodies.

Flow cytometry and sorting

Tumors were isolated and processed for fluorescence-activated cell sorting as previously described[14] using the following antibodies: CD31-FITC (1:100, BD Pharmingen, Franklin Lakes, NJ, USA), CD45-PE (1:200, BD Pharmingen), anti-F4/80-APC (1:100, Serotec) and DAPI for dead cell exclusion. The cells were sorted on a fluorescence-activated cell sorting Aria flow cytometer (BD Biosciences, San Jose, CA, USA) and several fractions collected: a mixed population of live cells (DAPI$^-$); purified tumor cells (DAPI$^-$ CD31$^-$CD45$^-$ F4/80$^-$); macrophages (DAPI$^-$ CD45$^+$ F4/80$^+$) and endothelial cells (DAPI$^-$ CD31$^+$).

RNA isolation and quantitative reverse transcriptase PCR

RNA was prepared from samples using TRIzol reagent and subsequently DNase-treated (Invitrogen) according to the manufacturers instructions. Complementary DNA was synthesized using the First Strand cDNA Synthesis Kit for reverse transcriptase PCR (Roche, Indianapolis, IN, USA). Real-time quantitative reverse transcriptase PCR was performed on complementary DNA samples using the ABI (Grand Island, NY, USA) 7900HT Fast Real-Time PCR system. Primers for ubiquitin C (Mm01201237_m1), CD68 (Mm03047343_m1), CD31 (Mm00476702_m1), heparanase (Mm00461768_m1), SV40 T-antigen (T-Ag, custom probe), LYVE-1 (Mm00475056_m1), podoplanin (Mm00494716_m1), VEGFR-1 (Mm00438980_m1), VEGFR-2 (Mm01222419_m1), VEGFR-3 (Mm01292604_m1), VEGF-A (Mm00437304_m1), VEGF-C (Mm01202432_m1), VEGF-D (Mm01131929_m1), FGF-2 (Mm00433287_m1), HGF (Mm01135193_m1), HPRT1 (Hs99999909_m1) and human heparanase (Hs00180737_m1) were purchased from Applied Biosystems (Grand Island, NY, USA).

Human PanNET samples

Two TMAs were constructed from archival paraffin-embedded tissue from a series of >150 PanNETs surgically resected from patients at Memorial Sloan-Kettering Cancer Center (MSKCC). Patient anonymity was ensured, and the study was performed in compliance with the Institutional Review Board. Three 0.6-mm tissue cores were punched from representative areas of the donor block and embedded in a recipient block using an automated TMA machine. Five-micrometer tissue sections were cut from this TMA and stained for heparanase and scored double-blindly by two authors (KEH and JAJ) as negative (0) or positive (three levels: weak (1); moderate (2); and strong (3)), based on staining intensity and percentage of cells that stained positive. Heparanase staining was then correlated to clinicopathological parameters including American Joint Cancer Committee tumor stage,[7] tumor grade (low: <2 mitoses/50 high-power field (HPF); intermediate: ⩾2 mitoses/50 HPF; and high grade: >50 mitoses/50 HPF)[8] and the number of mitoses per 50 HPFs scored by LHT. Samples with incomplete patient data

were excluded from the respective analysis. RNA was obtained from PanNETs in patient-matched primary and liver metastases as previously described.[29] Normal islet RNA was isolated from snap-frozen cultured human islets from healthy organ donors (Cell Transplant Center, Diabetes Research Institute, University of Miami School of Medicine).

Statistical analysis

Throughout this study, means $+/-$ s.e.m. are reported unless otherwise specified. For histological analyses of experimental animals, a subset of mice from each of the genotypes were selected at random. For all two-way comparisons, unpaired *t*-tests or Mann–Whitney tests were used as indicated and were considered statistically significant if $P<0.05$. A cumulative logit model[30] with generalized estimating equations to correct for correlations within individual mice was used to compare the distribution of tumor grades in RT2 mice. For TMA analysis of tumor stage, tumor grade and distant metastasis, Fisher's exact test was used. For comparison of mitosis, one-way analysis of variance was used.

CONFLICT OF INTEREST

The authors declare no conflict of interest.

ACKNOWLEDGEMENTS

We thank members of the Joyce Lab; Drs Jacqueline Bromberg and Andrew Koff for discussion on this topic; and Robert Bowman, Daniela Quail, Alberto Schuhmacher and Hao-Wei Wang for reading the manuscript. We gratefully acknowledge Xiaoping Chen and Lin Song for excellent technical assistance; Marsha Quick and Karoline Dubin for project assistance; Elyn Reidel, MSKCC Epidemiology and Biostatistics Department for statistical analysis of RT2 tumor grades; Sho Fujisawa and the Molecular Cytology Core Facility for assistance with the MetaMorph lymphangiogenesis analysis; the MSKCC Flow Cytometry Core for technical assistance and advice; and Aisha Khan of the cGMP Cell Processing Facility, Cell Transplant Center, Diabetes Research Institute, University of Miami School of Medicine for providing normal islets. This research was funded by the National Cancer Institute R01 CA125162 and Cycle for Survival (JAJ). KEH was supported in part by a Grayer Fellowship.

REFERENCES

1 Joyce JA, Pollard JW. Microenvironmental regulation of metastasis. *Nat Rev Cancer* 2009; **9**: 239–252.
2 Vlodavsky I, Beckhove P, Lerner I, Pisano C, Meirovitz A, Ilan N *et al.* Significance of heparanase in cancer and inflammation. *Cancer Microenvironment* 2012; **5**: 115–132.
3 Joyce JA, Freeman C, Meyer-Morse N, Parish CR, Hanahan D. A functional heparan sulfate mimetic implicates both heparanase and heparan sulfate in tumor angiogenesis and invasion in a mouse model of multistage cancer. *Oncogene* 2005; **24**: 4037–4051.
4 Yao JC, Eisner MP, Leary C, Dagohoy C, Phan A, Rashid A *et al.* Population-based study of islet cell carcinoma. *Ann Surg Oncol* 2007; **14**: 3492–3500.
5 Yao JC, Hassan M, Phan A, Dagohoy C, Leary C, Mares JE *et al.* One hundred years after "carcinoid": epidemiology of and prognostic factors for neuroendocrine tumors in 35,825 cases in the United States. *J Clin Oncol* 2008; **26**: 3063–3072.
6 Jiao Y, Shi C, Edil BH, de Wilde RF, Klimstra DS, Maitra A *et al.* DAXX/ATRX, MEN1, and mTOR pathway genes are frequently altered in pancreatic neuroendocrine tumors. *Science* 2011; **331**: 1199–1203.
7 Edge SB, Compton CC. The American Joint Committee on Cancer: the 7th edition of the AJCC cancer staging manual and the future of TNM. *Ann Surg Oncol* 2010; **17**: 1471–1474.
8 Ferrone CR, Tang LH, Tomlinson J, Gonen M, Hochwald SN, Brennan MF *et al.* Determining prognosis in patients with pancreatic endocrine neoplasms: can the WHO classification system be simplified? *J Clin Oncol* 2007; **25**: 5609–5615.
9 Nolan-Stevaux O, Truitt MC, Pahler JC, Olson P, Guinto C, Lee DC *et al.* Differential contribution to neuroendocrine tumorigenesis of parallel EGFR signaling in cancer cells and pericytes. *Genes Cancer* 2010; **1**: 125–141.
10 Tuveson D, Hanahan D. Translational medicine: cancer lessons from mice to humans. *Nature* 2011; **471**: 316–317.
11 Zcharia E, Jia J, Zhang X, Baraz L, Lindahl U, Peretz T *et al.* Newly generated heparanase knock-out mice unravel co-regulation of heparanase and matrix metalloproteinases. *PloS One* 2009; **4**: e5181.
12 Zcharia E, Metzger S, Chajek-Shaul T, Aingorn H, Elkin M, Friedmann Y *et al.* Transgenic expression of mammalian heparanase uncovers physiological functions of heparan sulfate in tissue morphogenesis, vascularization, and feeding behavior. *FASEB J* 2004; **18**: 252–263.
13 Lopez T, Hanahan D. Elevated levels of IGF-1 receptor convey invasive and metastatic capability in a mouse model of pancreatic islet tumorigenesis. *Cancer Cell* 2002; **1**: 339–353.
14 Pyonteck SM, Gadea BB, Wang HW, Gocheva V, Hunter KE, Tang LH *et al.* Deficiency of the macrophage growth factor CSF-1 disrupts pancreatic neuroendocrine tumor development. *Oncogene* 2012; **31**: 1459–1467.
15 Gocheva V, Wang HW, Gadea BB, Shree T, Hunter KE, Garfall AL *et al.* IL-4 induces cathepsin protease activity in tumor-associated macrophages to promote cancer growth and invasion. *Genes Dev* 2010; **24**: 241–255.
16 Mandriota SJ, Jussila L, Jeltsch M, Compagni A, Baetens D, Prevo R *et al.* Vascular endothelial growth factor-C-mediated lymphangiogenesis promotes tumour metastasis. *EMBO J* 2001; **20**: 672–682.
17 Zumsteg A, Christofori G. Myeloid cells and lymphangiogenesis. *Cold Spring Harb Perspect Med* 2012; **2**: a006494.
18 Zumsteg A, Baeriswyl V, Imaizumi N, Schwendener R, Ruegg C, Christofori G. Myeloid cells contribute to tumor lymphangiogenesis. *PloS One* 2009; **4**: e7067.
19 Maruyama K, Ii M, Cursiefen C, Jackson DG, Keino H, Tomita M *et al.* Inflammation-induced lymphangiogenesis in the cornea arises from CD11b-positive macrophages. *J Clin Invest* 2005; **115**: 2363–2372.
20 Tammela T, Alitalo K. Lymphangiogenesis: molecular mechanisms and future promise. *Cell* 2010; **140**: 460–476.
21 Parish CR, Freeman C, Brown KJ, Francis DJ, Cowden WB. Identification of sulfated oligosaccharide-based inhibitors of tumor growth and metastasis using novel in vitro assays for angiogenesis and heparanase activity. *Cancer Res* 1999; **59**: 3433–3441.
22 Ori A, Wilkinson MC, Fernig DG. A systems biology approach for the investigation of the heparin/heparan sulfate interactome. *J Biol Chem* 2011; **286**: 19892–19904.
23 Lindahl U, Li JP. Interactions between heparan sulfate and proteins-design and functional implications. *Int Rev Cell Mol Biol* 2009; **276**: 105–159.
24 Arvatz G, Shafat I, Levy-Adam F, Ilan N, Vlodavsky I. The heparanase system and tumor metastasis: is heparanase the seed and soil? *Cancer Metastasis Rev* 2011; **30**: 253–268.
25 Stenzel D, Nye E, Nisancioglu M, Adams RH, Yamaguchi Y, Gerhardt H. Peripheral mural cell recruitment requires cell-autonomous heparan sulfate. *Blood* 2009; **114**: 915–924.
26 Cohen-Kaplan V, Naroditsky I, Zetser A, Ilan N, Vlodavsky I, Doweck I. Heparanase induces VEGF C and facilitates tumor lymphangiogenesis. *Int J Cancer* 2008; **123**: 2566–2573.
27 Hanahan D. Heritable formation of pancreatic beta-cell tumours in transgenic mice expressing recombinant insulin/simian virus 40 oncogenes. *Nature* 1985; **315**: 115–122.
28 Okabe M, Ikawa M, Kominami K, Nakanishi T, Nishimune Y. 'Green mice' as a source of ubiquitous green cells. *FEBS Lett* 1997; **407**: 313–319.
29 Hu W, Feng Z, Modica I, Klimstra DS, Song L, Allen PJ *et al.* Gene Amplifications in well-differentiated pancreatic neuroendocrine tumors inactivate the p53 pathway. *Genes Cancer* 2010; **1**: 360–368.
30 Mccullagh P. Regression-models for ordinal data. *J Roy Stat Soc B Met* 1980; **42**: 109–142.

Supplementary Information accompanies this paper on the Oncogene website (http://www.nature.com/onc)